

Constraining the $\Lambda\Lambda$ interaction with terrestrial and astronomical data

Yusuke Tanimura,¹ Chang Ho Hyun,² and Myung-Ki Cheoun¹

¹*Department of Physics and Origin of Matter and Evolution of Galaxies (OMEG) Institute, Soongsil University, Seoul 06978, Korea*

²*Department of Physics Education, Daegu University, Gyeongsan 38453, Korea*
(Dated: February 23, 2026)

Terrestrial double- Λ hypernuclear data and astronomical observations of neutron stars provide complementary constraints on the $\Lambda\Lambda$ interaction. In this work, we investigate the $\Lambda\Lambda$ interaction within a Skyrme energy density functional framework based on the KIDS (Korea-IBS-Daegu-SKKU) models. We employ a Skyrme-type $\Lambda\Lambda$ interaction that includes the standard s - and p -wave terms, as well as a density-dependent term that effectively represents an $N\Lambda\Lambda$ three-body force. The s -wave terms are constrained using data on double- Λ hypernuclei supplemented by pseudodata obtained from core + 2Λ three-body model calculations including heavier hypernuclei. We show that the data on heavier systems are essential to simultaneously constrain the two s -wave parameters. We further explore the impact of the p -wave and $N\Lambda\Lambda$ components on the neutron-star properties and find that appropriate repulsive contributions of these terms yield consistency with current neutron-star mass-radius observations. These results indicate that the present framework provides phenomenologically acceptable equations of state for dense (N, Λ) matter over a wide range of densities and highlight the importance of future experimental data on heavier double- Λ hypernuclei.

I. INTRODUCTION

A standard scenario for the diversity of elements in the universe is that nuclei heavier than iron are created through the synthesis of radioactive isotopes far from the valley of stability and their decays in various modes. The synthesis of unstable nuclei is likely to occur in environments of extremely high density and temperature, such as supernova explosions and neutron-star mergers. Similarly, exotic particles and states that are absent in normal matter may appear at extreme conditions, and they can also play a critical role to form the present state of matter and universe. Hyperon is a well known example. Their production has been observed in relativistic heavy ion collisions [1–6], and their presence in neutron-star cores, though not directly measurable, is difficult to ignore in the current theoretical framework [7–20]. Accurate description of their physical properties and interactions with other particles will lead to deeper and wider understanding of the matter and the universe.

The tables compiled by the Particle Data Group [21] show that the basic properties of the lightest hyperons in the baryon octet are measured at high precision. Their interactions with the nucleon are relatively well understood by means of numerous experimental data and theoretical studies within various microscopic approaches [22–27]. Interactions between hyperons, on the other hand, are poorly constrained. In Ref. [28], interactions between Λ hyperons (hereafter referred to as $\Lambda\Lambda$ interaction) were described in the form of Skyrme force that contains five unknown parameters. At that time the only experimental information available to constrain the $\Lambda\Lambda$ interaction was the binding energy of ${}^{13}_{\Lambda\Lambda}\text{B}$. The two key parameters [λ_0 and λ_1 in our notation in Eq. (4)] were fit to the this datum, while the remaining three parameters (λ_2 , λ_3 and α) were set to zero. Resulting interaction had large uncertainty and consequent neutron star equation

of state (EoS) at high densities ranged from soft to stiff regions.

Almost thirty years have passed since Ref. [28] was published. In the meantime, there were progress in the experiment for the double Λ hypernuclei. The number of data has increased and their accuracy has been improved. In this work, we examine to what extent the $\Lambda\Lambda$ interactions can be constrained by using the hypernuclear data and neutron-star properties obtained from the astronomical measurements.

There have been numerous theoretical efforts to investigate the effects of the $\Lambda\Lambda$ interactions, particularly in the context of the hyperon puzzle associated with $\approx 2M_{\odot}$ neutron stars. Such studies have been carried out within Skyrme-type frameworks [7–11] as well as other theoretical models [9, 11–20]. The $\Lambda\Lambda$ force has also been used in studies of multi- Λ hypernuclei [29–46].

Very recently, an attempt has been made in Ref. [10] to constrain the parameters of the Skyrme-type $\Lambda\Lambda$ interaction based on the data from double- Λ hypernuclei and astronomical observations. By systematically employing a Bayesian framework, the authors provided simultaneous constraints on the five parameters including those associated with effective $\Lambda\Lambda$ and $N\Lambda\Lambda$ interactions.

In this work, we adopt a complementary approach. While we also make use of both hypernuclear data and neutron-star observations, the former is supplemented by pseudodata obtained from core + 2Λ three-body model calculations for heavier systems. The three-body model is constructed to be consistent with the existing data for single- Λ hypernuclei and for the double- Λ hypernucleus ${}^6_{\Lambda\Lambda}\text{He}$ [47, 48]. This framework allows us to separate the sensitivities of the parameters to different datasets: the s -wave parameters are well constrained by the hypernuclear information, whereas the remaining parameters are explored using the neutron-star observables.

We find that the s -wave Skyrme parameters λ_0 and

λ_1 cannot be determined uniquely with the three data of binding energies for ${}_{\Lambda\Lambda}^{11}\text{Be}$, ${}_{\Lambda\Lambda}^9\text{Li}$ and ${}_{\Lambda\Lambda}^9\text{Be}$. When four pseudodata for ${}_{\Lambda\Lambda}^{18}\text{O}$, ${}_{\Lambda\Lambda}^{34}\text{S}$, ${}_{\Lambda\Lambda}^{42}\text{Ca}$ and ${}_{\Lambda\Lambda}^{58}\text{Ni}$ are included, these parameters become significantly better constrained within a narrow region. However, the seven data are insufficient to constrain the density-dependence parameter λ_3 , so the fitting is not able to determine even its sign. To further constrain λ_3 as well as the p -wave parameter λ_2 , we examine their impact on the neutron-star maximum mass and mass-radius relation. Although the resulting neutron-star properties exhibit some dependence on the underlying symmetry energy, the combination of medium-mass double- Λ hypernuclear information and neutron-star properties provides meaningful constraints on these parameters.

The paper is organized as follows. In Sec. II, we describe the energy density functional for $\Lambda\Lambda$ interaction adopted in this work. The results and discussions are presented in Sec. III. Section IV summarizes the present study and provides an outlook. Details of the three-body model are given in the Appendix A.

II. MODEL: SKYRME ENERGY DENSITY FUNCTIONAL

The KIDS model [49, 50] is a Skyrme-type energy density functional (EDF) for multi- Λ hypernuclear systems, written as

$$E = \int d^3r \mathcal{E}, \quad (1)$$

where the total energy density is decomposed into three contributions,

$$\mathcal{E} = \mathcal{E}_{NN} + \mathcal{E}_{N\Lambda} + \mathcal{E}_{\Lambda\Lambda}. \quad (2)$$

Here, \mathcal{E}_{NN} is the nucleonic energy density [49], $\mathcal{E}_{N\Lambda}$ includes the kinetic energy density of Λ hyperons and the effective $N\Lambda$ interaction [50], and $\mathcal{E}_{\Lambda\Lambda}$ represents the $\Lambda\Lambda$ interaction.

The $\Lambda\Lambda$ contribution adopted in this work is given by

$$\begin{aligned} \mathcal{E}_{\Lambda\Lambda} = & \frac{1}{4}\lambda_0\rho_\Lambda^2 + \frac{1}{8}(\lambda_1 + 3\lambda_2)\rho_\Lambda\tau_\Lambda \\ & + \frac{3}{32}(\lambda_2 - \lambda_1)\rho_\Lambda\nabla^2\rho_\Lambda + \frac{1}{4}\lambda_3\rho_\Lambda^2\rho_N, \end{aligned} \quad (3)$$

where ρ_Λ and τ_Λ are the number density and the kinetic-energy density of Λ hyperons, respectively, and ρ_N is the total nucleon density. This EDF is based on a Skyrme-type effective $\Lambda\Lambda$ interaction of Ref. [28]:

$$\begin{aligned} v_{\Lambda\Lambda} = & \left[\lambda_0 + \lambda_3\rho_N^\alpha \left(\frac{\mathbf{r}_1 + \mathbf{r}_2}{2} \right) \right] \delta(\mathbf{r}_1 - \mathbf{r}_2) \\ & - \frac{\lambda_1}{8} \left[\overleftarrow{\nabla}^2 \delta(\mathbf{r}_1 - \mathbf{r}_2) + \delta(\mathbf{r}_1 - \mathbf{r}_2) \overrightarrow{\nabla}^2 \right] \\ & + \frac{\lambda_2}{4} \overleftarrow{\nabla} \cdot \delta(\mathbf{r}_1 - \mathbf{r}_2) \overrightarrow{\nabla}, \end{aligned} \quad (4)$$

with $\alpha = 1$. Here, $\overrightarrow{\nabla} = \nabla_1 - \nabla_2$ acts on the right, while $\overleftarrow{\nabla} = \nabla_1 - \nabla_2$ acts on the left. Given the limited amount of information available on the $\Lambda\Lambda$ interaction, we fix $\alpha = 1$ to reduce the number of free parameters. The remaining coefficients λ_i ($i = 0 - 3$) are treated as adjustable parameters. The terms with λ_0 and λ_1 are the s -wave interactions, while the λ_2 term is the p -wave one [28, 51]. The density-dependent λ_3 term introduces an effective repulsive $N\Lambda\Lambda$ three-body force.

All the Hartree-Fock calculations with the KIDS functional in the present work are done by imposing the spherical symmetry and the equal-filling approximation.

III. RESULTS AND DISCUSSIONS

A. Double- Λ hypernuclei: fitting of λ_0 and λ_1

In the present work, we employ the KIDS functionals (KIDS0, KIDS-A, KIDS-B, KIDS-C, and KIDS-D) for the NN sector [49]. For the $N\Lambda$ sector we employ the Y4 parameter sets [50] corresponding to each NN parameter set. The remaining $\Lambda\Lambda$ interaction parameters should then be adjusted to available experimental data. However, the data on double- Λ hypernuclei are limited to light systems and insufficient to fully constrain all the parameters in Eq. (3).

Therefore, in the first step, we try to constrain only λ_0 and λ_1 of the s -wave terms. The p -wave interaction terms proportional to λ_2 are excluded because their contribution vanishes identically for the ground states of double- Λ systems, in which the two Λ particles occupy the $1s$ orbital [28]. The density-dependent term involving λ_3 is left unconstrained as it is sensitive mainly to variation of strange matter properties as a function of the density. A discussion of the resulting high-density equation of state will be presented later.

Even the simultaneous determination of λ_0 and λ_1 is challenging when only very light double- Λ hypernuclei are considered. The parameter λ_0 mainly reflects bulk nuclear properties, whereas λ_1 is more sensitive to surface effects. Therefore, a reliable determination of both parameters ideally requires data covering systems with different mass numbers, since the balance between bulk and surface contributions varies with system size. To this end, we supplement the limited experimental information with pseudodata for heavier double- Λ hypernuclei obtained from a core + 2Λ three-body model, which is constructed to be consistent with the existing data for single- Λ hypernuclei and ${}_{\Lambda\Lambda}^6\text{He}$ (see Appendix A for details).

The parameters λ_0 and λ_1 will be determined by fitting to the experimental binding energies of double- Λ hypernuclei. The single- and double- Λ binding energies of

TABLE I. The dataset used to fit the $\Lambda\Lambda$ interaction parameters λ_0 and λ_1 . The values shown in boldface are included in the dataset, and the pseudodata are marked with an asterisk. The value $B_{\Lambda\Lambda}$ for ${}^{11}_{\Lambda\Lambda}\text{Be}$ is experimental [52], whereas those for ${}^9_{\Lambda\Lambda}\text{Li}$ and ${}^9_{\Lambda\Lambda}\text{Be}$ are taken from four-body cluster model calculations in Ref. [53]. The four pseudodata for $\Delta B_{\Lambda\Lambda}$ of heavier systems with $A \geq 18$ are obtained from the three-body model calculations presented in Appendix A.

Nuclide	$\Delta B_{\Lambda\Lambda}$ (MeV)	$B_{\Lambda\Lambda}$ (MeV)
${}^{11}_{\Lambda\Lambda}\text{Be}$ [52]	—	19.07
${}^9_{\Lambda\Lambda}\text{Li}$ [53]	—	14.55*
${}^9_{\Lambda\Lambda}\text{Be}$ [53]	—	14.40*
${}^{18}_{\Lambda\Lambda}\text{O}$	1.22*	27.30*
${}^{34}_{\Lambda\Lambda}\text{S}$	1.07*	36.42*
${}^{42}_{\Lambda\Lambda}\text{Ca}$	1.00*	39.03*
${}^{58}_{\Lambda\Lambda}\text{Ni}$	0.86*	42.60*

hypernuclei are defined as

$$B_{\Lambda}({}^A_{\Lambda}Z) = B({}^AZ) - B({}^{A-1}Z), \quad (5)$$

$$B_{\Lambda\Lambda}({}^A_{\Lambda\Lambda}Z) = B({}^A_{\Lambda\Lambda}Z) - B({}^{A-2}Z), \quad (6)$$

respectively, where B denotes the total binding energy of a nucleus. We also introduce the two- Λ correlation energy:

$$\Delta B_{\Lambda\Lambda}({}^A_{\Lambda\Lambda}Z) = B_{\Lambda\Lambda}({}^A_{\Lambda\Lambda}Z) - 2B_{\Lambda}({}^{A-1}Z), \quad (7)$$

which is predominantly sensitive to the $\Lambda\Lambda$ interaction.

The model parameters are optimized by minimizing the mean absolute relative deviation (MD),

$$\text{MD} = \frac{1}{N_{\text{data}}} \sum_{i=1}^{N_{\text{data}}} \left| \frac{O_i^{\text{calc}} - O_i^{\text{expt}}}{O_i^{\text{expt}}} \right|, \quad (8)$$

where N_{data} is the number of data points, O_i^{expt} and O_i^{calc} are the experimental and calculated values of the observable i , respectively.

Table I summarizes the dataset employed for the fitting of the parameters λ_0 and λ_1 . We use an experimental value of $B_{\Lambda\Lambda}$ for ${}^{11}_{\Lambda\Lambda}\text{Be}$ reported in Ref. [52], the calculated $B_{\Lambda\Lambda}$ values of ${}^9_{\Lambda\Lambda}\text{Li}$ and ${}^9_{\Lambda\Lambda}\text{Be}$ from Ref. [53], and four more pseudodata for $\Delta B_{\Lambda\Lambda}$ of ${}^{18}_{\Lambda\Lambda}\text{O}$, ${}^{34}_{\Lambda\Lambda}\text{S}$, ${}^{42}_{\Lambda\Lambda}\text{Ca}$, and ${}^{58}_{\Lambda\Lambda}\text{Ni}$. The pseudodata for $A \geq 18$ are obtained from the three-body model calculations performed in this work.

We perform two-parameter fittings with $\lambda_2 = \lambda_3 = 0$. The parameter sets are labeled as “KIDS(0/-A/-B/-C/-D)-Y4-LL2” or, if not confusing, “LL2” for short. Figure 1 shows the MD values [Eq. (8)] as functions of the $\Lambda\Lambda$ interaction parameters λ_0 and λ_1 for (a) dataset restricted to ${}^{11}_{\Lambda\Lambda}\text{Be}$, ${}^9_{\Lambda\Lambda}\text{Li}$, and ${}^9_{\Lambda\Lambda}\text{Be}$ and (b) the full set

given in Tab. I. Here, KIDS0 and KIDS0-Y4 parameter sets are used for NN and $N\Lambda$ interactions, respectively. As seen in Fig. 1(a), the dataset restricted to the light systems is insufficient to determine both parameters simultaneously. The MD landscape exhibits an elongated

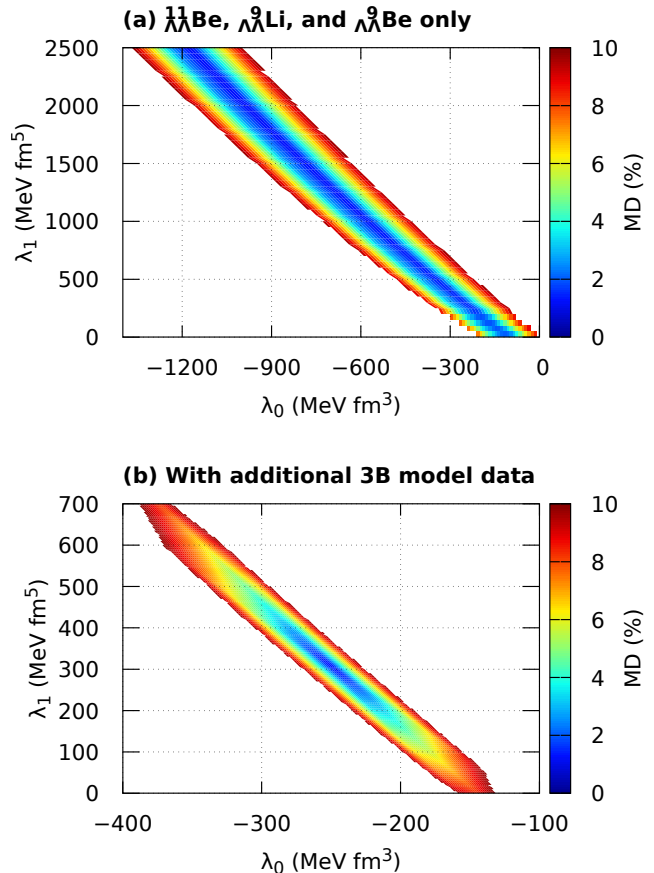


FIG. 1. MD values defined in Eq. (8) as functions of the $\Lambda\Lambda$ interaction parameters λ_0 and λ_1 for (a) the restricted dataset consisting of ${}^{11}_{\Lambda\Lambda}\text{Be}$, ${}^9_{\Lambda\Lambda}\text{Li}$, and ${}^9_{\Lambda\Lambda}\text{Be}$, and (b) the full dataset listed in Table I. The remaining parameters are fixed at $\lambda_2 = 0$ and $\lambda_3 = 0$. KIDS0 and KIDS0-Y4 parameter sets are used for NN and $N\Lambda$ interactions, respectively.

valley in the (λ_0, λ_1) plane, effectively constraining only a quasi-linear combination of the two parameters. In contrast, Fig. 1(b) shows that the full dataset, which includes heavier systems, provides a well-defined minimum and thus enables a more reliable and simultaneous determination of both λ_0 and λ_1 . This confirms the preceding argument that a dataset covering a wide range of mass numbers is essential for simultaneously constraining the bulk and surface components of the functional. Table II summarizes the LL2 parameter sets obtained by minimizing the MD value for the full dataset.

Table III compares between data and calculated values for $B_{\Lambda\Lambda}$ and $\Delta B_{\Lambda\Lambda}$ for nuclei included in the dataset. The sets LL2 reproduce the dataset reasonably well, especially the $\Delta B_{\Lambda\Lambda}$ pseudodata. This is reasonable given that the

TABLE II. Parameter sets in the $\Lambda\Lambda$ sector obtained from fittings to full dataset in Table I together with the corresponding MD values. The Y4 parameter sets are employed for the $N\Lambda$ sector [50]. The LL2 series, in which $\lambda_2 = \lambda_3 = 0$, are listed.

	KIDS0	KIDS-A	KIDS-B	KIDS-C	KIDS-D
	LL2	LL2	LL2	LL2	LL2
λ_0 (MeV fm ³)	-249.32	-232.01	-246.31	-253.39	-240.61
λ_1 (MeV fm ⁵)	305.70	268.19	300.40	314.53	286.95
λ_2 (MeV fm ⁵)	0	0	0	0	0
λ_3 (MeV fm ⁶)	0	0	0	0	0
MD (%)	1.13	2.80	1.49	0.89	2.45

TABLE III. Comparison between data and calculated values for $B_{\Lambda\Lambda}$ and $\Delta B_{\Lambda\Lambda}$ in unit of MeV.

Observables	Data	KIDS0	KIDS-A	KIDS-B	KIDS-C	KIDS-D
		LL2	LL2	LL2	LL2	LL2
$B_{\Lambda\Lambda}$ (${}_{\Lambda\Lambda}^{11}\text{Be}$)	19.07	18.37	17.78	18.24	18.44	17.89
$B_{\Lambda\Lambda}$ (${}_{\Lambda\Lambda}^9\text{Li}$)	14.55	14.45	13.70	14.22	14.55	13.87
$B_{\Lambda\Lambda}$ (${}_{\Lambda\Lambda}^9\text{Be}$)	14.40	14.44	13.67	14.19	14.53	13.85
$\Delta B_{\Lambda\Lambda}$ (${}_{\Lambda\Lambda}^{18}\text{O}$)	1.22	1.22	1.22	1.22	1.22	1.22
$\Delta B_{\Lambda\Lambda}$ (${}_{\Lambda\Lambda}^{34}\text{S}$)	1.07	1.08	1.07	1.08	1.07	1.08
$\Delta B_{\Lambda\Lambda}$ (${}_{\Lambda\Lambda}^{42}\text{Ca}$)	1.00	0.98	0.99	0.99	0.99	0.98
$\Delta B_{\Lambda\Lambda}$ (${}_{\Lambda\Lambda}^{58}\text{Ni}$)	0.86	0.86	0.87	0.86	0.87	0.86

mean-field theory is suitable to heavier systems.

We try also three-parameter (λ_0 , λ_1 , and λ_3) fits to the full dataset. These parameter sets are labeled “KIDS(0/-A/-B/-C/-D)-Y4-LL3” or “LL3” for short. Table IV summarizes the LL3 parameter sets obtained by minimizing the MD value for the full dataset. The inclusion of the λ_3 term does not lead to any significant improvement in the quality of the fit. We have also examined fits with λ_3 fixed at positive values and found that excessively large values of λ_3 deteriorate the agreement with the hypernuclear data, which constrains λ_3 only loosely (see next subsection).

These results suggest that the density-dependent $\Lambda\Lambda$

TABLE IV. LL3 Parameter sets in the $\Lambda\Lambda$ sector obtained from fittings to full dataset in Table I together with the corresponding MD values. The Y4 parameter sets are employed for the $N\Lambda$ sector [50].

	KIDS0	KIDS-A	KIDS-B	KIDS-C	KIDS-D
	LL3	LL3	LL3	LL3	LL3
λ_0 (MeV fm ³)	-272.14	-222.29	-261.12	-238.01	-253.72
λ_1 (MeV fm ⁵)	321.23	257.48	309.48	295.96	294.50
λ_2 (MeV fm ⁵)	0	0	0	0	0
λ_3 (MeV fm ⁶)	119.06	-35.82	79.93	-54.57	70.19
MD (%)	0.96	2.77	1.35	0.83	2.32

interaction plays a secondary role in finite hypernuclei (at least for the systems included in the present dataset) but becomes relevant for dense matter. Additional information, such as constraints from neutron-star observables, is therefore required to further restrict λ_3 as well as λ_2 , which is irrelevant to the ground states of hypernuclei.

B. (λ_2, λ_3) dependence of neutron-star properties

In this section, we investigate the (λ_2, λ_3) dependence of neutron-star properties within the present models. We explore the parameter space of λ_2 and λ_3 by requiring that the maximum mass of neutron stars exceeds $2M_\odot$ [54–58] and that the mass-radius (M-R) relation agrees with the NICER data for PSR J0740+6620 [59, 60]. To this end, stellar configurations are obtained by solving the Tolman-Oppenheimer-Volkov (TOV) equation for a given EoS of neutron-star matter.

The EoSs for homogeneous $n\rho e\mu$ or $n\rho\Lambda e\mu$ matter in cold and neutrino-free neutron stars are constructed using the KIDS models under the conditions of charge neutrality and β equilibrium [12]. The crust EoSs for low densities are taken from Refs. [61, 62]. The transition to the KIDS EoS for homogeneous matter is made at a mass density of 1.5×10^{14} g/cm³, following Ref. [63]. To examine the causality of the EoSs, we evaluate the speed

of sound, defined as

$$c_s^2 = \frac{dP}{d\varepsilon}, \quad (9)$$

where P is the pressure given as a function of the energy density ε obtained from an EoS. If the speed of sound exceeds the speed of light at any density reached in a neutron-star configuration obtained from the TOV equations, the corresponding stellar configuration is excluded from the M-R plot.

We focus on KIDS-A and KIDS-D models together with the corresponding hyperonic functionals. Hereafter, we simultaneously include all the four parameters of $\mathcal{E}_{\Lambda\Lambda}$ in our consideration and label the parameter sets by “KIDS-(A/D)-Y4-LL4(λ_2, λ_3)” or simply “LL4(λ_2, λ_3)”, where λ_2 and λ_3 are specified in units of MeV fm^5 and MeV fm^6 , respectively.

The LL4(λ_2, λ_3) parameter sets are constructed as follows. For a given value of λ_3 , the parameters λ_0 and λ_1 are refitted to the data listed in Tab. I for the double- Λ hypernuclei. We consider $\lambda_3 = 0, 100, 200, \dots$ MeV fm^6 and impose an upper bound on λ_3 by the resulting MD value, requiring that it does not exceed the minimum MD value for the LL3 set shown in Tab. IV by more than 1%. This practical criterion of the 1% threshold is motivated by the fact that the pseudodata for $\Delta B_{\Lambda\Lambda} \sim 1$ MeV are specified to three significant digits. Nevertheless, this choice is to some extent arbitrary. The resulting upper bounds of λ_3 are found to be ~ 700 MeV fm^6 for KIDS-A and ~ 1000 MeV fm^6 for KIDS-D. See Fig. 2 for the optimized values of (λ_0, λ_1) for different values of λ_3 ranging from 0 to its upper bound. The squares and circles represent the results for KIDS-A-Y4-LL4(\ast, λ_3) and KIDS-D-Y4-LL4(\ast, λ_3), respectively, and the color indicates the value of λ_3 . (Tables of all parameter sets examined in this study are provided in the Supplemental Materials.) As discussed in the previous subsection, λ_2 is irrelevant to the ground-state properties of double- Λ hypernuclei. Accordingly, for a given value of λ_3 and a given KIDS model (A or D), the values of λ_0 and λ_1 are common to all values of λ_2 .

Figures 3 and 4 show (a) the M-R relations, (b) the speed of sound as a function of the baryon density ρ_B , and (c) the fraction of Λ hyperons at the centers of neutron stars as a function of stellar mass, which are obtained with EoSs of KIDS-A-Y4-LL4($\lambda_2, 0$) and KIDS-D-Y4-LL4($\lambda_2, 0$) models, respectively, with λ_2 ranging from 0 to 600 MeV fm^5 . Here, the density-dependent term is turned off ($a_3 = 0$). In these figures, the black-dashed curves represent the results obtained with nucleonic-matter EoSs without Λ hyperons, while the colored curves correspond to hyperonic-matter EoSs. Each M-R curve is terminated at the point where the causality condition is violated anywhere inside the star. Filled circles indicate the maximum mass configurations when they are reached before the causality limit. The light-blue regions enclosed by solid and dashed lines indicate the 1σ and 2σ credible regions, respectively, of NICER

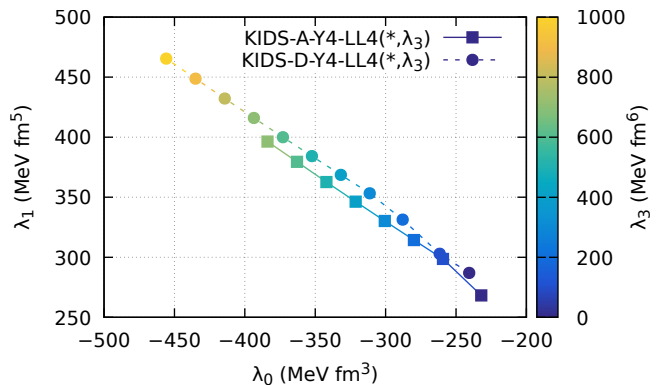


FIG. 2. Values of (λ_0, λ_1) determined by fittings to hypernuclear data with λ_3 fixed at 0, 100, 200, \dots MeV fm^6 . The squares and circles represent the results for KIDS-A and -D, respectively, and the color indicates the value of λ_3 . The upper bounds of λ_3 is determined by the MD values. See main texts for detail.

data for PSR J0740+6620 [59, 60]. For each of the KIDS-A and KIDS-D models, the corresponding Y4 parameter set is adopted for the $N\Lambda$ sector.

As seen in Figs. 3(a) and 4(a), for the both KIDS models without hyperons, the maximum neutron-star mass exceeds $2M_\odot$. When hyperons are included with $\lambda_2 = 0$, however, the EoSs become significantly softer, and the maximum mass is reduced to values below $2M_\odot$, illustrating a so-called hyperon puzzle. This behavior can be understood from the corresponding speed-of-sound curves shown in Figs. 3(b) and 4(b). As seen in the violet ($\lambda_2 = 0$) curves, the emergence of the new baryonic degree of freedom at densities $\rho_B \approx 0.4 - 0.5 \text{ fm}^{-3}$ softens the EoS, and this softening persists up to high densities of $\rho_B \sim 1.5 \text{ fm}^{-3}$. For $\lambda_2 > 0$, the speed-of-sound curves indicate a recovery of stiffness due to the additional $\Lambda\Lambda$ repulsion. Consequently, the maximum neutron-star mass exceeds $2M_\odot$ for $\lambda_2 \gtrsim 300 \text{ MeV fm}^5$ in the KIDS-A models, and for $\lambda_2 \gtrsim 100 \text{ MeV fm}^5$ in the KIDS-D models. For sufficiently large values of λ_2 , the M-R curves also pass through the 2σ or 1σ credible regions of the NICER observation for PSR J0740+6620. However, the M-R curves tend to saturate as λ_2 increases, and the maximum mass as well converges to $(2.0 - 2.2)M_\odot$, making it difficult to infer an upper bound of λ_2 by the present neutron-star M-R observables alone. Note that the scan over λ_2 is similar to that performed by Togashi et al. [18], who investigated the impact of the p -wave $\Lambda\Lambda$ interaction on neutron-star properties by varying its strength within a finite-range potential model. What is observed here is qualitatively similar to their results.

The relative fractions of Λ hyperons at the centers of neutron stars, $Y_{\Lambda,c}$, are shown in Figs. 3(c) and 4(c). For the maximum-mass neutron stars, we find $Y_{\Lambda,c} \approx 0.6 - 0.7$ for $\lambda_2 = 0$, whereas $Y_{\Lambda,c} \approx 0.2 - 0.3$ for $\lambda_2 = 600 \text{ MeV fm}^5$ in both models. Within the present framework, the central Λ -hyperon fraction in massive neutron stars is typi-

cally found to be $Y_\Lambda \sim 0.2 - 0.3$.

Figure 5 summarizes the neutron-star properties in the (λ_2, λ_3) plane for (a) KIDS-A and (b) KIDS-D. The figure indicates whether the neutron-star mass exceeds $2M_\odot$ and whether the M-R curve passes through the credible region of NICER data for PSR J0740+6620. The colored and filled points in the (λ_2, λ_3) plane may be regarded phenomenologically acceptable. As discussed earlier, the parameter λ_3 is bounded from above by the double- Λ hypernuclear data, whereas an upper bound of λ_2 cannot be determined from the neutron-star observables alone in the present analyses. Within the explored parameter domain, the conditions from the present neutron-star observables on the M-R relation for massive neutron stars are more sensitive to λ_2 than to λ_3 . The repulsive effect of $\lambda_3 > 0$, below its upper bound, slightly shifts the M-R curves upward for $M \gtrsim 2M_\odot$, reducing the threshold value of λ_2 by at most $\sim 100 \text{ MeV fm}^5$.

As a final remark, we compare the present results with those of Ref. [10]. From Figs. 2 and 5, the acceptable parameter ranges in the present analysis can be approximately summarized as $-500 \lesssim \lambda_0 \lesssim -200 \text{ (MeV fm}^3\text{)}$, $250 \lesssim \lambda_1 \lesssim 500 \text{ (MeV fm}^5\text{)}$, $100 \lesssim \lambda_2 \lesssim 600 \text{ (MeV fm}^5\text{)}$, and $0 \leq \lambda_3 \lesssim 1000 \text{ (MeV fm}^6\text{)}$, where we restrict the discussion to $\lambda_3 \geq 0$. Comparison with the posterior distributions reported in Ref. [10] indicates that the allowed regions for λ_0 and λ_1 show marginal overlap. A remarkable agreement is found for the p -wave parameter λ_2 , whose maximum-likelihood value in Ref. [10] falls within our acceptable range. This consistency can be attributed to the fact that λ_2 is constrained solely by neutron-star properties in both frameworks. The agreement for the density-dependent parameter λ_3 is less pronounced. These differences can be understood in terms of the different inputs adopted in the two analyses. In particular, the present study relies on hypernuclear information supplemented by pseudodata spanning a wider mass range, whereas Ref. [10] uses the potential depth inferred from a limited set of light double- Λ hypernuclear data and also treats the exponent α of the density-dependent term as an additional free parameter. We note that Ref. [10] obtains informative posterior distributions within the prior ranges they adopted, indicating that their datasets provide meaningful constraints on the $\Lambda\Lambda$ interaction. Taken together, the two studies underscore the complementary roles of hypernuclear and astrophysical information in constraining the $\Lambda\Lambda$ interaction.

IV. CONCLUSIONS AND OUTLOOK

In this work, we have investigated the $\Lambda\Lambda$ interaction in finite nuclei and dense matter within a Skyrme energy density functional framework based on the KIDS models. A Skyrme-type $\Lambda\Lambda$ interaction including the standard s - and p -wave terms, as well as a density-dependent contribution representing an effective $N\Lambda\Lambda$ three-body force, has been employed. The primary goal of this study was to

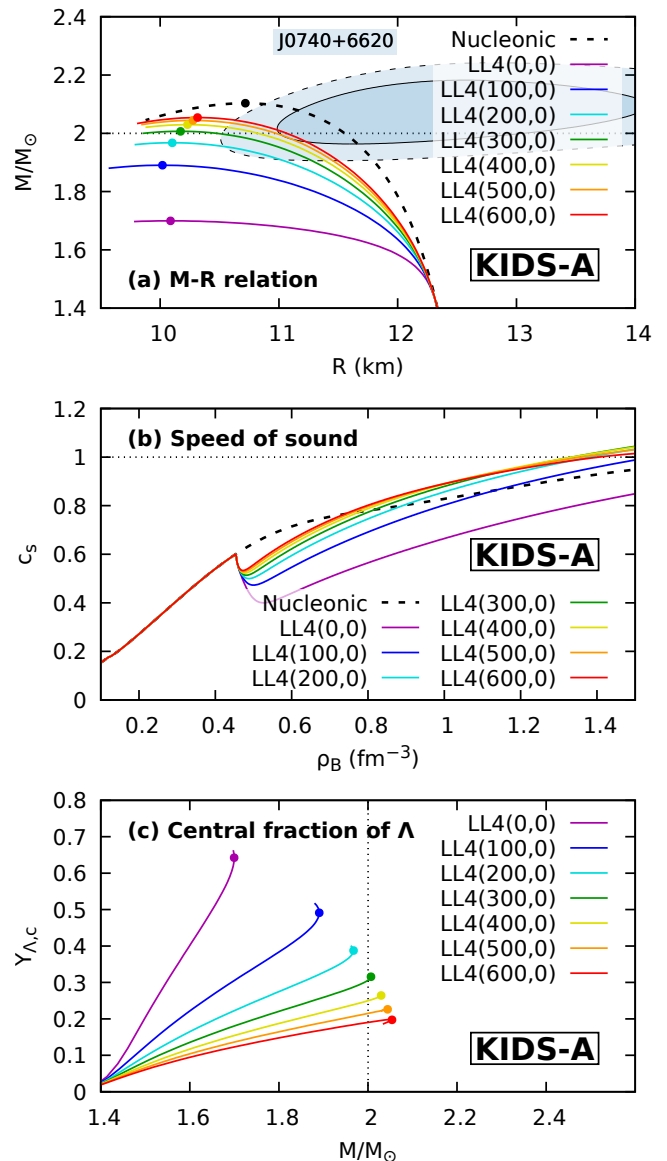


FIG. 3. (a) Mass-radius (M-R) relations of neutron stars calculated with different EoSs. The black-dashed curve corresponds to nucleonic matter (KIDS-A), while the colored curves show the results for hyperonic matter based on the KIDS-A + KIDS-A-Y4 + KIDS-A-Y4-LL4($\lambda_2, 0$) models. Each curve is terminated at the central density where the causality condition is violated anywhere inside the star. Filled circles indicate the maximum-mass configurations when they are reached before the causality limit. The light-blue regions enclosed by solid and dashed lines indicate the 1σ and 2σ credible regions, respectively, of NICER data for PSR J0740+6620 [59, 60]. (b) Speed of sound as a function of the baryon density for the corresponding EoSs. (c) Fraction of Λ hyperons at the centers of neutron stars as a function of stellar mass.

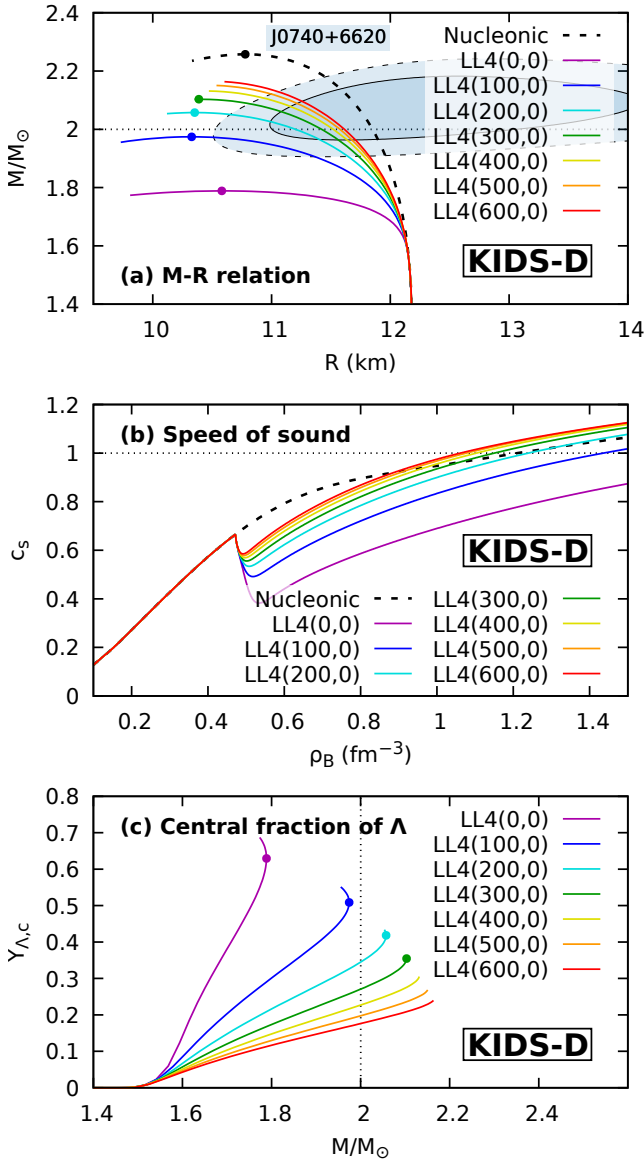


FIG. 4. Same as Fig. 3 but for KIDS-D model.

constrain the poorly known $\Lambda\Lambda$ interaction by combining information from double- Λ hypernuclei and astronomical observations of neutron stars.

Using the available experimental data for light double- Λ hypernuclei together with pseudodata obtained from core + 2Λ three-body model calculations, we have shown that the inclusion of heavier systems is essential for a simultaneous and reliable determination of the bulk and surface components of the $\Lambda\Lambda$ interaction. In particular, the parameters associated with the s -wave terms, λ_0 and λ_1 , can be constrained within a relatively narrow range once the pseudodata for medium-mass hypernuclei are included. The resulting parameter sets reproduce the available double- Λ binding energies and $\Lambda\Lambda$ correlation energies with good accuracy.

We have further explored the roles of the p -wave $\Lambda\Lambda$ in-

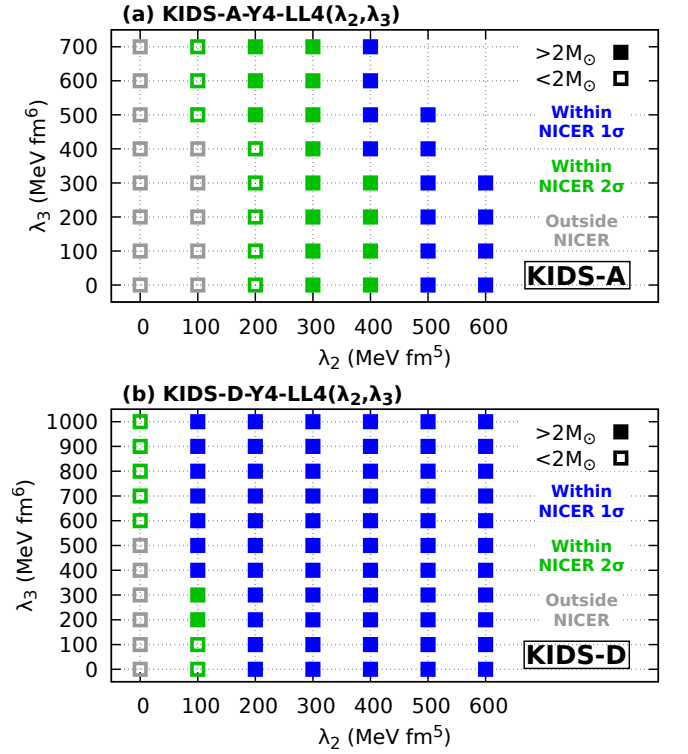


FIG. 5. Summary of the neutron-star properties in the (λ_2, λ_3) plane for (a) KIDS-A-Y4-LL4 (λ_2, λ_3) and (b) KIDS-D-Y4-LL4 (λ_2, λ_3) parameter sets. Closed and open symbols indicate whether or not the maximum neutron-star mass exceeds $2M_\odot$. The consistency of the M-R curves with the NICER data for PSR J0740+6620 [59, 60] is distinguished by colors: consistent within 1σ ; green: consistent within 2σ ; gray: outside the 2σ region).

teraction and the density-dependent $N\Lambda\Lambda$ term by examining neutron-star properties. The emergence of Λ hyperons softens the EoS and reduces the maximum neutron-star mass below $2M_\odot$ when these repulsive components are absent. However, we have demonstrated that a moderate repulsion provided by the p -wave term, and to a lesser extent by the density-dependent term, restores sufficient stiffness of the EoS, allowing the EoS to be consistent with the observed masses and radii of massive neutron stars, including the NICER constraints for PSR J0740+6620. Within the phenomenologically acceptable parameter region, the central Λ -hyperon fraction in massive neutron stars is typically found to be $Y_{\Lambda,c} \sim 0.2 - 0.3$.

The present results indicate that the KIDS-based Skyrme energy density functional, augmented by a suitably constrained $\Lambda\Lambda$ interaction, provides a coherent description of both multi- Λ hypernuclei and hyperonic neutron-star matter. The present analysis also highlights the importance of systematic measurements of double- Λ hypernuclei over a wide mass range, which would provide direct constraints on the $\Lambda\Lambda$ interaction complementary to astrophysical observations. Future experimental data

on heavier double- Λ hypernuclei and improved astronomical constraints on neutron-star observables will be crucial for further refining the $\Lambda\Lambda$ and $N\Lambda\Lambda$ interactions and for achieving a more definitive resolution of the hyperon puzzle.

The present $\Lambda\Lambda$ interaction can serve as a starting point for systematic Skyrme EDF studies of double- and multi- Λ hypernuclei, including their ground-state properties [39, 41, 43, 45, 64] or the collective properties [36–38]. Applying the present dataset within relativistic mean-field frameworks based on flavor SU(3) symmetry [12, 16, 17, 34], which include additional hyperons such as Σ and Ξ , would also be an interesting direction for future work.

ACKNOWLEDGMENTS

We are grateful to Emiko Hiyama for providing us the numerical GEM code for three-body calculations and for valuable discussions on the $\Lambda\Lambda$ interaction and its impact on double- Λ hypernuclei. Y. T. thanks Tsuyoshi Miyatsu for helpful discussions on neutron-star equations of state and related observables. Y. T. acknowledges support from the Basic Science Research Program of the National Research Foundation of Korea (NRF) under grants No. RS-2024-00361003, RS-2024-00460031, and RS-2021-NR060129. C. H. H. is grateful to Hana Gil for the discussions on the neutron-star mass-radius relation. Work of C. H. H. was supported by the NRF research grant No. 2023R1A2C1003177. Work of M. K. C. was supported by the NRF research grant No. RS-2025-16071941.

Appendix A: Three-body model

To generate pseudodata for $\Delta B_{\Lambda\Lambda}$, we employ a core + 2Λ three-body model for double- Λ hypernuclei. The Hamiltonian is given by

$$H_{3B} = \frac{\mathbf{P}_c^2}{2M_c} + \sum_{i=1,2} \left[\frac{\mathbf{p}_i^2}{2m_\Lambda} + V_{c\Lambda}(|\mathbf{r}_i - \mathbf{r}_c|) \right] + v_{\Lambda\Lambda}(|\mathbf{r}_1 - \mathbf{r}_2|) - T_{CM}, \quad (\text{A1})$$

where M_c and \mathbf{P}_c are the mass and the momentum of the core normal nucleus, \mathbf{p}_i ($i = 1, 2$) is the momentum of the i th Λ hyperon, $V_{c\Lambda}$ and $v_{\Lambda\Lambda}$ denote the core- Λ and $\Lambda\Lambda$ interactions, and T_{CM} is the center-of-mass (CM) kinetic energy.

The three-body Schrödinger equation is solved using the Gaussian expansion method (GEM) [65, 66]. To describe the ground state with $J^\pi = 0^+$, only s -wave components are taken into account for the relative motions defined by the Jacobi coordinates. The core is treated as a spinless particle.

TABLE V. The measured binding energies (MeV) of Λ included in the fitting of WS parameters. The data are taken from Refs. [22, 67].

Nuclide	s orbit	p orbit	d orbit	f orbit	g orbit
${}_{\Lambda}^{16}\text{O}$	12.5 ± 0.35	2.5 ± 0.35			
${}_{\Lambda}^{32}\text{S}$	17.5 ± 0.5	8.1 ± 0.6			
${}_{\Lambda}^{40}\text{Ca}$	18.7 ± 1.1	11.0 ± 0.6	1.0 ± 0.5		
${}_{\Lambda}^{208}\text{Pb}$	26.3 ± 0.8	21.9 ± 0.6	16.8 ± 0.7	11.7 ± 0.6	6.6 ± 0.6

TABLE VI. Optimal values of the WS parameters obtained by the fitting.

$V_{c\Lambda}^0$ (MeV)	r_0 (fm)	a (fm)
-30.1506	1.1264	0.6789

1. Core-Lambda potential

The core- Λ potential is determined so as to reproduce the empirical single- Λ binding energies B_Λ . The binding energy is given by the solution of the Schrödinger equation for the relative motion,

$$\left[-\frac{\hbar^2}{2\mu} \nabla^2 + V_{c\Lambda}(r) \right] \varphi(\mathbf{r}) = -B_\Lambda \varphi(\mathbf{r}), \quad (\text{A2})$$

where $\mu = M_c m_\Lambda / (M_c + m_\Lambda)$ is the reduced mass. The core mass is taken as $M_c = (A - 1)m_N$, with $m_N = (m_n + m_p)/2 = 938.918754$ MeV, and the mass of Λ is taken to be $m_\Lambda = 1115.68$ MeV [21].

We adopt a core- Λ potential of a Woods-Saxon (WS) type:

$$V_{c\Lambda}(r) = \frac{V_{c\Lambda}^0}{1 + \exp[(r - R)/a]}, \quad R = r_0(A - 1)^{1/3}. \quad (\text{A3})$$

The three parameters $V_{c\Lambda}^0$, r_0 , and a are fitted to the measured B_Λ values of ${}_{\Lambda}^{16}\text{O}$, ${}_{\Lambda}^{32}\text{S}$, and ${}_{\Lambda}^{40}\text{Ca}$, and ${}_{\Lambda}^{208}\text{Pb}$ (see Table V). The optimal parameters are listed in Table VI. A comparison between calculated and experimental B_Λ values is shown in Fig. 6.

a. ${}^4\text{He}$ - Λ folding potential

The WS potential determined above is not suitable for the light system ${}_{\Lambda}^5\text{He}$ and fails to reproduce the B_Λ value of 3.12 MeV [68]. For ${}_{\Lambda}^5\text{He}$ we instead use an α - Λ folding potential.

The $N\Lambda$ potential is taken as a one-range-Gaussian,

$$v_{N\Lambda}(r) = v_{N\Lambda}^0 (1 + \eta \boldsymbol{\sigma}_N \cdot \boldsymbol{\sigma}_\Lambda) e^{-r^2/\beta_{N\Lambda}^2}, \quad (\text{A4})$$

with the parameters $\beta_{N\Lambda} = 1.034$ fm and $\eta = -0.1$ [69]. The strength $v_{N\Lambda}^0$ will be determined below.

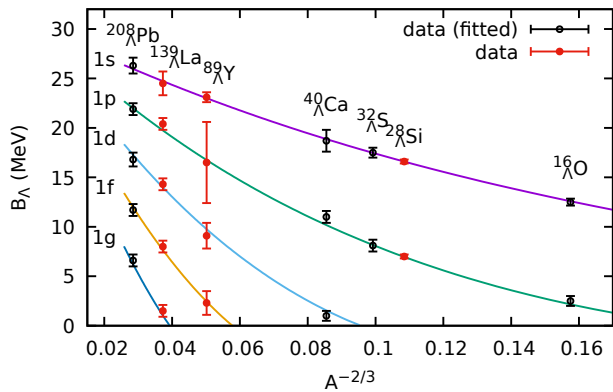


FIG. 6. Comparison of B_Λ 's between the WS-potential model and the data. The black symbols denote experimental data included in the fit, whereas the red symbols denote those not included in the fit.

TABLE VII. Parameters of the ${}^4\text{He}-\Lambda$ folding potential. The oscillator length μ_α is refitted to reproduce the measured charge radius of ${}^4\text{He}$. The strength $v_{N\Lambda}^0$ is refitted to reproduce $B_\Lambda({}^5_\Lambda\text{He}) = 3.12$ MeV.

$\mu_\alpha^{-1/2}$ (fm)	$\beta_{N\Lambda}$ (fm)	$v_{N\Lambda}^0$ (MeV)
1.366	1.034	-38.39

The α particle is described as a $(1s)^4$ harmonic-oscillator configuration. Its intrinsic density (after the center-of-mass correction) is given by

$$\rho_\alpha(\mathbf{r}) = 4 \left(\frac{4\mu_\alpha}{3\pi} \right)^{3/2} e^{-\frac{4}{3}\mu_\alpha r^2}, \quad (\text{A5})$$

where $\mu_\alpha^{-1/2}$ is the oscillator length. The parameter μ_α is adjusted so that the charge radius

$$r_{\text{ch}} = \sqrt{\frac{9}{8\mu_\alpha} + 0.841^2 \text{ fm}^2}, \quad (\text{A6})$$

where the proton size of 0.841 fm is quoted from PDG [21], matches the measured value, 1.6755(28) fm [70]. A value $1/\mu_\alpha = 1.366^2 \text{ fm}^2$ yields $r_{\text{ch}} = 1.6753$ fm.

The $\alpha\Lambda$ folding potential is then given by [71]

$$\begin{aligned} V_{\alpha\Lambda}(r) &= \int d^3r' \rho_\alpha(\mathbf{r}') v_{N\Lambda}(|\mathbf{r} - \mathbf{r}'|) \\ &= 4v_{N\Lambda}^0 \left(\frac{4\mu_\alpha}{4\mu_\alpha + 3\mu_v} \right)^{3/2} \exp\left(-\frac{4\mu_\alpha\mu_v}{4\mu_\alpha + 3\mu_v} r^2\right), \end{aligned} \quad (\text{A7})$$

where $\mu_v \equiv 1/\beta_{N\Lambda}^2$. To reproduce $B_\Lambda = 3.12$ MeV, $v_{N\Lambda}^0$ is readjusted to -38.39 MeV. The resulting parameters in $V_{\alpha\Lambda}$ are summarized in Table VII.

TABLE VIII. Parameters of the $\Lambda\Lambda$ interaction taken from Ref. [53]. In the present three-body model calculation, the overall factor of $f_{\Lambda\Lambda} = 0.9685$ is applied to make a fine readjustment (see main texts).

i	μ_i (fm $^{-2}$)	v_i (MeV)	v_i^σ (MeV)
1	0.555	-10.67	0.0966
2	1.656	-93.51	16.08
3	8.163	4884	915.8

TABLE IX. Calculated values of the $\Lambda\Lambda$ correlation energy $\Delta B_{\Lambda\Lambda}$, the double- Λ binding energy $B_{\Lambda\Lambda}$, and the Λ binding energy B_Λ of the corresponding single- Λ nucleus. Note that $\Delta B_{\Lambda\Lambda}({}^A_{\Lambda\Lambda}Z) = B_{\Lambda\Lambda}({}^A_{\Lambda\Lambda}Z) - 2B_\Lambda({}^{A-1}_\Lambda Z)$.

Hypernucleus	$\Delta B_{\Lambda\Lambda}$ (MeV)	$B_{\Lambda\Lambda}$ (MeV)	B_Λ (${}^{A-1}_\Lambda Z$) (MeV)
${}^6_{\Lambda\Lambda}\text{He}$	0.67	6.91	3.12
${}^{18}_{\Lambda\Lambda}\text{O}$	1.22	27.30	13.04
${}^{34}_{\Lambda\Lambda}\text{S}$	1.07	36.42	17.67
${}^{42}_{\Lambda\Lambda}\text{Ca}$	1.00	39.03	19.02
${}^{58}_{\Lambda\Lambda}\text{Ni}$	0.86	42.60	20.87

2. Lambda-Lambda potential

For the $\Lambda\Lambda$ interaction we use a three-range Gaussian potential of [53],

$$v_{\Lambda\Lambda}(r) = \sum_{i=1}^3 (v_i + v_i^\sigma \boldsymbol{\sigma}_\Lambda \cdot \boldsymbol{\sigma}_\Lambda) e^{-\mu_i r^2}. \quad (\text{A8})$$

The parameters used in Ref. [53] are listed in Table VIII. To reproduce $B_{\Lambda\Lambda} = 6.91$ MeV of NAGARA event [47, 48] using the present three-body model (see App. A 1a), the potential is multiplied by an overall renormalization factor,

$$v_{\Lambda\Lambda} \rightarrow f_{\Lambda\Lambda} v_{\Lambda\Lambda}, \quad f_{\Lambda\Lambda} = 0.9685. \quad (\text{A9})$$

Using the core- Λ and the $\Lambda\Lambda$ interactions thus obtained, we perform three-body model calculations for several double hypernuclei. The resulting pseudodata for $B_{\Lambda\Lambda}$ and $\Delta B_{\Lambda\Lambda}$ are summarized in Table IX. The values of $\Delta B_{\Lambda\Lambda}$ for ${}^{18}_{\Lambda\Lambda}\text{O}$, ${}^{34}_{\Lambda\Lambda}\text{S}$, ${}^{42}_{\Lambda\Lambda}\text{Ca}$, and ${}^{58}_{\Lambda\Lambda}\text{Ni}$ are used to constrain the $\Lambda\Lambda$ part of the functional in the main analysis.

- [1] STAR Collaboration, Experimental and theoretical challenges in the search for the quarkgluon plasma: The STAR Collaboration’s critical assessment of the evidence from RHIC collisions, *Nucl. Phys.* **A757**, 102 (2005).
- [2] ALICE Collaboration, Multi-strange baryon production at mid-rapidity in Pb-Pb collisions at $\sqrt{s_{NN}} = 2.76$ TeV, *Phys. Lett.* **B728**, 216 (2014).
- [3] ALICE Collaboration, ${}^3_{\Lambda}\text{H}$ and ${}^3_{\Lambda}\bar{\text{H}}$ production in Pb-Pb collisions at $\sqrt{s_{NN}} = 2.76$ TeV, *Phys. Lett.* **B754**, 360 (2016).
- [4] ALICE Collaboration, Measurement of ${}^3_{\Lambda}\text{H}$ Production in Pb-Pb collisions at $\sqrt{s_{NN}} = 5.02$ TeV, *Phys. Lett.* **B860**, 139066 (2025).
- [5] ALICE Collaboration, $\bar{\Sigma}^{\pm}$ production in pp and p-Pb collisions at $\sqrt{s_{NN}} = 5.02$ TeV, *Eur. Phys. J. C* **86**, 132 (2026).
- [6] Z.-Q. Feng, Extracting the hyperon-nucleon interaction via collective flows in heavy-ion collisions, *Phys. Lett.* **B851** 138580 (2024).
- [7] L. Mornas, Neutrons stars in a Skyrme model with hyperons, *Eur. Phys. J. A* **24**, 293 (2005).
- [8] Yeunhwan Lim, Chang Ho Hyun, Kyujin Kwak, and Chang-Hwan Lee, Hyperon puzzle of neutron stars with Skyrme force models, *Int. J. Mod. Phys. E* **24**, 1550100 (2015).
- [9] Debarati Chatterjee and Isaac Vidaña, Do hyperons exist in the interior of neutron stars?, *Eur. Phys. J. A* **52**, 29 (2016).
- [10] X. D. Sun, S. C. Han, J. N. Hu, A. Li, Exploring Hyperon Skyrme Forces in Multi- Λ Hypernuclei and Neutron Star Matter, arXiv:2602.03388 [nucl-th] (2026).
- [11] M. Oertel, M. Hempel, T. Klähn, and S. Typel, Equations of state for supernovae and compact stars, *Rev. Mod. Phys.* **89**, 015007 (2017).
- [12] Norman K. Glendenning, “Compact Stars: Nuclear Physics, Particle Physics, and General Relativity”, 2nd ed. (Springer-Verlag New York, 2000).
- [13] Domenico Logoteta, Hyperons in Neutron Stars, *Universe* **2021**, 7, 408 (2021).
- [14] H.-J. Schulze, A. Polls, A. Ramos, and I. Vidaña, Maximum mass of neutron stars, *Phys. Rev. C* **73**, 058801 (2006).
- [15] H.-J. Schulze, T. Rijken, Maximum mass of hyperon stars with the Nijmegen ESC08 model, *Phys. Rev. C* **84**, 035801 (2011).
- [16] Tsuyoshi Miyatsu and Myung-Ki Cheoun, and Koichi Saito, Equation of state for neutron stars in SU(3) flavor symmetry, *Phys. Rev. C* **88**, 015802 (2013).
- [17] Tsuyoshi Miyatsu, Myung-Ki Cheoun, Kyungsik Kim, and Koichi Saito, Equation of State for Hyperonic Neutron-Star Matter in SU(3) Flavor Symmetry, *Symmetry* **2025**, 17, 1872 (2025).
- [18] H. Togashi, E. Hiyama, Y. Yamamoto, and M. Takano, Equation of state for neutron stars with hyperons using a variational method, *Phys. Rev. C* **93**, 035808 (2016).
- [19] Y. Yamamoto, H. Togashi, T. Tamagawa, T. Furumoto, N. Yasutake, and Th. A. Rijken, *Phys. Rev. C* **96**, 065804 (2017).
- [20] A. Mohammad Ali Looee, M. Shahrbaaf, and H. R. Moshfegh, Hyperons in Neutron Stars across the Observed Mass Range: Insights from ΛN and $\Lambda\Lambda$ Interactions within a Microscopic Framework, *Astrophys. J.* **997**, 26 (2026).
- [21] S. Navas *et al.*, Review of Particle Physics, *Phys. Rev. D* **110**, 030001 (2022).
- [22] O. Hashimoto and H. Tamura, Spectroscopy of Λ hypernuclei, *Prog. Part. Nucl. Phys.* **57**, 264 (2006).
- [23] A. Feliciello and T. Nagae, Experimental review of hypernuclear physics: recent achievements and future perspectives, *Rep. Prog. Phys.* **78**, 096301 (2015).
- [24] Elena Botta, Tullio Bressani, and Gianni Garbarino, Strangeness nuclear physics: a critical review on selected topics, *Eur. Phys. J. A* **48**, 41 (2012).
- [25] B. F. Gibson, E. V. Hungerford III, A survey of hypernuclear physics, *Phys. Rep.* **257**, 349 (1995).
- [26] A. Gal, E. V. Hungerford, and D. J. Millener, Strangeness in nuclear physics, *Rev. Mod. Phys.* **88**, 035004 (2016).
- [27] Stefan Petschauer, Johann Haidenbauer, Norbert Kaiser, Ulf-G. Meißner, and Wolfram Weise, Hyperon-Nuclear Interactions From SU(3) Chiral Effective Field Theory *Front. Phys.* **8**, 12 (2020).
- [28] D. E. Lancscoy, Double- Λ hypernuclei in the Skyrme-Hartree-Fock approach and nuclear core polarization, *Phys. Rev. C* **58**, 3351 (1998).
- [29] Hiroharu Bandō, Kiyomi Ikeda, and Toshio Motoba, Hypernuclear Cluster Structure: – Di-“Lambpha” System –, *Prog. Theor. Phys.* **66**, 1344 (1981); Hiroharu Bandō, Kiyomi Ikeda, and Toshio Motoba, Microscopic Study of Lambpha ($\alpha_{\Lambda} \equiv {}^6_{\Lambda\Lambda}\text{He}$) and Di- α_{Λ} Cluster States, *Prog. Theor. Phys.* **67**, 508 (1982).
- [30] Koichi Miyahara, Kiyomi Ikeda, and Hiroharu Bando, Molecular Orbital Model Study of the ${}^9_{\Lambda}\text{Be}$, ${}^{10}_{\Lambda\Lambda}\text{Be}$, ${}^{11}_{3\Lambda}\text{Be}$, and ${}^{12}_{4\Lambda}\text{Be}$ Hypernuclei, *Prog. Theor. Phys.* **69**, 1717 (1983).
- [31] Kiyomi Ikeda, Hiroharu Bandō, Toshio Motoba, Multi-Strange Hypernuclei, *Prog. Theor. Phys. Suppl.*, **81**, 147 (1985).
- [32] M. Rufa, J. Schaffner, J. Maruhn, H. Stöcker, W. Greiner, and P.-G. Reinhard, Multi-lambda hypernuclei and the equation of state of hypermatter, *Phys. Rev. C* **42**, 2469 (1990); Erratum, *Phys. Rev. C* **43**, 2020 (1991).
- [33] J. Mareš and J. Žofka, Multi-strange systems in relativistic mean fields, *Z. Phys. A* **345**, 47 (1993).
- [34] J. Schaffner, C. B. Dover, A. Gal, C. Greiner, D. J. Millener, and H. Stöcker, Multiply Strange Nuclear Systems, *Ann. Phys.* **235**, 35 (1994).
- [35] Emiko Hiyama, Masayasu Kamimura, Yasuo Yamamoto, Toshio Motoba and Thomas A. Rijken, $S = -2$ Hypernuclear Structure, *Prog. Theor. Phys. Suppl.* **185**, 152, (2010).
- [36] F. Minato and K. Hagino, Application of random-phase approximation to vibrational excitations of double- Λ hypernuclei, *Phys. Rev. C* **85** 024316 (2012).
- [37] F. Minato, S. Chiba, and K. Hagino, Fission of heavy Λ hypernuclei with the Skyrme-Hartree-Fock approach, *Nucl. Phys.* **A831**, 150 (2009).
- [38] F. Minato and S. Chiba, Fission barrier of actinide nuclei with double- Λ particles within the Skyrme-Hartree-Fock method, *Nucl. Phys.* **A856**, 55 (2011).
- [39] E. Khan, J. Margueron, F. Gulminelli, and Ad. R. Raduta, Microscopic evaluation of the hypernuclear chart with Λ hyperons, *Phys. Rev. C* **92**, 044313 (2015).

- [40] J. Margueron, E. Khan, and F. Gulminelli, Density Functional approach for multistrange hypernuclei: Competition between Λ and $\Xi^{0,-}$ hyperons, *Phys. Rev. C* **96**, 054317 (2017).
- [41] H. Güven, K. Bozkurt, E. Khan, and J. Margueron $\Lambda\Lambda$ pairing in multistrange hypernuclei, *Phys. Rev. C* **98**, 014318 (2018).
- [42] Yusuke Tanimura, Clusterization and deformation of multi- Λ hypernuclei within a relativistic mean-field model, *Phys. Rev. C* **99**, 034324, (2019).
- [43] Jing Guo, C. F. Chen, Xian-Rong Zhou, Q. B. Chen, and H.-J. Schulze, $\Lambda\Lambda$ pairing effects in spherical and deformed multi- Λ hyperisotopes, *Phys. Rev. C* **105**, 034322 (2022).
- [44] Bahruz Suleymanli, Kutsal Bozkurt, Elias Khan, Haşim Güven, Jérôme Margueron, Effects of finite temperature and pairing correlations in multi- Λ hypernuclei, *Phys. Rev. C* **110**, 014329 (2024).
- [45] Ying Zhang, Emiko Hiyama, and Hiroyuki Sagawa, $\Lambda\Lambda$ interaction in multi- Λ hypernuclei of O and Ca isotopes *Eur. Phys. J. A* **61**, 278 (2025).
- [46] Xin Li, C. F. Chen, Xian-Rong Zhou, and Zhongzhou Ren, Clusterization and localization of multi- Λ hyperisotopes, *Phys. Rev. C* **109**, 064301 (2024).
- [47] J. K. Ahn *et al.*, Double- Λ hypernuclei observed in a hybrid emulsion experiment, *Phys. Rev. C* **88** 014003 (2013).
- [48] H. Takahashi *et al.*, Observation of a ${}^6_{\Lambda\Lambda}\text{He}$ Double Hypernucleus, *Phys. Rev. Lett.* **87**, 212502 (2001).
- [49] Hana Gil, Nobuo Hinohara, Chang Ho Hyun, and Kenichi Yoshida, KIDS density functional for deformed nuclei: examples of the even-even Nd isotopes, *J. Korean Phys. Soc.* **81**, 113-120 (2022).
- [50] Soonchul Choi, Emiko Hiyama, Chang Ho Hyun, and Myung-Ki Cheoun, Effects of many-body interactions in hypernuclei with Korea-IBS-Daegu-SKKU functionals, *Eur. Phys. J. A* **58**, 161 (2022).
- [51] D. Vautherin and D. M. Brink, Hartree-Fock Calculations with Skyrme's Interaction. I. Spherical Nuclei, *Phys. Rev. C* **5**, 626 (1972).
- [52] H. Ekawa *et al.*, Observation of a Be double-Lambda hypernucleus in the J-PARC E07 experiment, *Prog. Theor. Expt. Phys.*, **2019**, 021D02 (2019).
- [53] E. Hiyama, M. Kamimura, T. Motoba, T. Yamada, and Y. Yamamoto, Four-body cluster structure of $A = 7-10$ double- Λ hypernuclei, *Phys. Rev. C* **66**, 024007 (2002).
- [54] P. B. Demorest, T. Pennucci, S. M. Ransom, M. S. E. Roberts, J. W. T. Hessels, A two-solar-mass neutron star measured using Shapiro delay, *Nature* **467**, 1081 (2010).
- [55] Zaven Arzumanyan *et al.*, The NANOGrav 11-year Data Set: High-precision Timing of 45 Millisecond Pulsars, *Astrophys. J. Suppl.* **235**, 37 (2016).
- [56] J. Antoniadis *et al.*, A Massive Pulsar in a Compact Relativistic Binary, *Science* **340**, 1233232 (2013).
- [57] H. T. Cromartie, Relativistic Shapiro delay measurements of an extremely massive millisecond pulsar, *Nat. Astron.* **4**, 72 (2020).
- [58] E. Fonseca *et al.*, Refined Mass and Geometric Measurements of the High-mass PSR J0740+6620, *Astrophys. J. Lett.* **915**, L12 (2021).
- [59] Tuomo Salmi *et al.*, The Radius of the High-mass Pulsar PSR J0740+6620 with 3.6 yr of NICER Data, *Astrophys. J.* **974**, 294 (2024).
- [60] Tuomo Salmi *et al.*, Data and Software for: 'The Radius of the High-mass Pulsar PSR J0740+6620 with 3.6 yr of NICER Data', Version 1.0.0, Zenodo (2024).
- [61] Gordon Baym, Christopher Pethick, and Peter Sutherland, The Ground State of Matter at High Densities: Equation of State and Stellar Models, *Astrophys. J.* **170**, 299 (1971).
- [62] Gordon Baym, Hans A. Bethe, and Christopher J. Pethick, Neutron Star Matter, *Nucl. Phys.* **A175**, 225 (1971).
- [63] E. Chabanat, P. Bonche, P. Haensel, J. Meyer, and R. Schaeffer, A Skyrme parametrization from subnuclear to neutron star densities, *Nucl. Phys.* **A627**, 710 (1997).
- [64] J. Cugnon, A. Lejeune, and H.-J. Schulze, Hypernuclei in the Skyrme-Hartree-Fock formalism with a microscopic hyperon-nucleon force, *Phys. Rev. C* **62**, 064308 (2000).
- [65] E. Hiyama, Y. Kino, M. Kamimura, Gaussian expansion method for few-body systems, *Prog. Part. Nucl. Phys.* **51**, (2003).
- [66] Emiko Hiyama, Gaussian expansion method for few-body systems and its applications to atomic and nuclear physics, *Prog. Theor. Exp. Phys.*, **2012**, 01A204, (2012).
- [67] Q. N. Usmani and A. R. Bodmer, Λ single particle energies, *Phys. Rev. C* **60**, 055215 (1999).
- [68] M. Jurić *et al.*, A new determination of the binding-energy values of the light hypernuclei ($A \leq 15$), *Nucl. Phys.* **B52**, 1 (1973).
- [69] Toshio Motoba, Hiroharu Bandō, Kiyomi Ikeda, and Taiichi Yamada, Chapter III. Production, Structure and Decay of Light p -Shell Λ -Hypernuclei, *Prog. Theor. Phys. Suppl.* **81**, 42 (1985).
- [70] I. Angeli and K.P. Marinova, Table of experimental nuclear ground state charge radii: An update, *At. Data Nucl. Data Tables* **99**, 69 (2013).
- [71] Emiko Hiyama, Masayasu Kamimura, Toshio Motoba, Taiichi Yamada, and Yasuo Yamamoto, Three- and Four-Body Cluster Models of Hypernuclei Using the G-Matrix ΛN Interaction: ${}^9_{\Lambda}\text{Be}$, ${}^{13}_{\Lambda}\text{C}$, ${}^6_{\Lambda\Lambda}\text{He}$ and ${}^{10}_{\Lambda\Lambda}\text{Be}$, *Prog. Theor. Phys.* **97**, 881 (1997).